**International Journal of Applied Mathematics**

**Volume 38 No. 5, 2025**

ISSN: 1311-1728 (printed version); ISSN: 1314-8060 (on-line version)

# MUON SITE ESTIMATION OF $CERU_2AL_{10}$ AT GROUND STATE STUDIED BY DENSITY FUNCTIONAL THEORY

**Noraina Adam[1*,2], Saidah Sakinah Mohd Tajudin[1,2], Edi Suprayoga[1,3], Mohamed Ismail Mohamed-Ibrahim[2] and Shukri Sulaiman[2], Isao Watanabe[1]**

[1*]Advanced Meson Science Laboratory, RIKEN Nishina Center, Wako, Saitama 351-0198, Japan

[2]Computational Chemistry and Physics Laboratory, Universiti Sains Malaysia, 11700 Penang, Malaysia

[3]Physics Department, Institut Teknologi Bandung, Jl. Ganesha 10, Bandung, Jawa Barat, 40132, Indonesia

***Corresponding author:** Noraina Adam

*E-mail: norainaadam5724@gmail.com Telephone number: +609-7677583 ORCID ID : 0009-0002-2990-0750

**Abstract**

We presented our investigation on the muon site estimation in metallic ground state of antiferromagnetic $CeRu_2Al_{10}$ by using the density functional theory (DFT). In this calculation, we estimated the position of muon site using local spin density approximation (LSDA) and the pseudopotential technique of plane-wave approximation adopted from Vienna Ab-initio Software Package (VASP). We calculated the dipole field by using the internal field from $\mu$SR experimental analysis as our reference in order to gain more understanding on the electronic properties of $CeRu_2Al_{10}$ at the muon site. Two positions of muon site were estimated, and the dipole fields were converged to 21.5 G and 150 G. The hybridization of the system was observed through the distribution of charge density. From our observations, we suggested that the two internal fields sensed by positive muon came from dynamic and static magnetic fields that arise from hybridization and ordered magnetic moments.

**Keywords:** DFT; Metallic Ground State; Kondo Semiconductor; $CeRu_2Al_{10}$; c-*f* Hybridization, Magnetic

## 1.0 Introduction

The compound $YbFe_2Al_{10}$-type $CeM_2Al_{10}$ ($M$ = Ru, Os) has been reported to be a Kondo semiconductor due to the formation of spin gap at low temperature [1, 2] and at the same time, the compound also exhibits a long-range antiferromagnetic order at ground state [3, 4]. A spin gap was spotted in $CeRu_2Al_{10}$ and $CeOs_2Al_{10}$ below the $T_0$ by the inelastic neutron scattering (INS) at 8 meV and 11 meV, respectively [1, 2]. In terms of the gap opening, the semiconducting behaviour of $CeRu_2Al_{10}$ was expected to be close to $CeFe_2Al_{10}$ compared to $CeOs_2Al_{10}$ since Fe, Ru, and Os are in the order of 3d, 4d, and 5d system, respectively [4, 5, 6]. However, the electric resistivity measurement observed a vice versa characteristic between

Received: August 04, 2025

**International Journal of Applied Mathematics**

**Volume 38 No. 5, 2025**

ISSN: 1311-1728 (printed version); ISSN: 1314-8060 (on-line version)

$CeRu_2Al_{10}$ and $CeOs_2Al_{10}$. The semiconducting behaviour in $CeOs_2Al_{10}$ continued until low temperature while in $CeRu_2Al_{10}$, the thermal activation-type at low temperature disappeared due to the metallic behaviour [7, 8]. After pressure was applied, the $T_0$ of both systems increased. It was unusual compared to other Kondo semiconductor related to the Ce-ion such as CeNiSn, where the $T_0$ decreased by pressures due to the suppression of RKKY interaction by the Kondo effect [8, 9]. The ground state of $CeRu_2Al_{10}$ turned to semiconductor after 2 GPa was applied while the $CeOs_2Al_{10}$ exhibited the metallic ground state [3]. The result suggested that the $CeOs_2Al_{10}$ was approaching more to Kondo semiconductor in a valence fluctuation regime compared to $CeRu_2Al_{10}$ and it was supported by the $^{27}Al$ NQR measurement of $CeOs_2Al_{10}$ [10, 11, 12].

The ground state of $CeRu_2Al_{10}$ was also investigated using the muon spin relaxation ($\mu$SR) [13, 14]. The first study was done by Khalyavin *et. al*. where long-range magnetic order was observed at $T_0$ at two internal fields, ~30 G and ~120 G [13]. However, another study by Kambe *et al* found only an internal field which was 30 G [14]. Meanwhile, the $\mu$SR analysis by Guo *et.al* found the internal field of $CeRu_2Al_{10}$ to be ~178G and 30 G which possibly due to the type of sample [15]. The internal field was governed by the hyperfine interaction between the positive muons ($\mu^+$) and the magnetic moments at the muon site. The muon sites have been estimated by Adroja *et al* [16] and Kambe *et. al* [14] which were at (0, 0, 0) and (0.5, 0, 0.25), two fractional atomic coordinates of a unit cell. However, no further study has been done to investigate the electronic structure around the muon sites.

In order to gain further information on the hyperfine interaction field in the metallic ground state of $CeRu_2Al_{10}$, we performed a density functional theory (DFT) calculation using the Vienna Ab-initio Simulation Package (VASP) [17, 18, 19] by using the internal field analysis from the $\mu$SR experiments as our references [13, 14, 15].

## 2.0 Calculation Methods

### 2.1 Band Structure Calculation

In order to simulate the antiferromagnetic and metallic ground state of $CeRu_2Al_{10}$, we performed the calculations by using the local spin density approximation (LSDA) without adding the Hubbard parameter, U. It is understandable that Hubbard parameter is usually added for calculation involving strong correlated system. However, since $CeRu_2Al_{10}$ was regarded as an unusual and easily perturbed strong correlated system, we tried to observe the minimum standard DFT calculation first without additional parameter. The calculation adopted the standard pseudopotential technique of plane-wave approximation implemented by Vienna ab-initio software package (VASP). In the case of CeRu2Al10 where the valence electron could easily change the behaviour of the compound, the standard PAW pseudopotential was used for each atom instead of ultrasoft pseudopotential [20]. The calculation began with investigating the electronic band structure and the density of state (DOS) of $CeRu_2Al_{10}$ before estimating the muon site position. It started with the self-consistent field (SCF) calculation which was done on a unit cell with ENCUT = 300 eV, ISPIN = 2, PREC = Accurate, ICHARG = 2 and standard

Received: August 04, 2025

International Journal of Applied Mathematics
Volume 38 No. 5, 2025
ISSN: 1311-1728 (printed version); ISSN: 1314-8060 (on-line version)

Monkhorst-Pack mesh for k-points. After that, CHGCAR from SCF calculation was carried into the non-SCF calculation where the INCAR file was set as IBRION = -1, NSW = 0, ICHARG = 11 to obtain the band structure with k-points along the strings where high symmetry points of the Brillouin zone were connected [21].

The crystal structure of $CeRu_2Al_{10}$ was an orthorhombic $YbFe_2Al_{10}$-type structure with space group *Cmcm* (63) and Z = 4 formula units per unit cell. The lattice parameters of the unit cell $CeRuAl_{10}$ were $a$ = 9.18 Å, $b$ = 10.28 Å and $c$ = 9.12 Å and the unit cell volume, $V$ = 0.8615 $nm^3$. The atoms in $CeRu_2Al_{10}$ were coordinated in seven crystallographic sites where Ce in *4c*, Ru or Os in *8d*, two Al atoms in *8g*, two Al atoms in *8f* and one Al in *8e* [22, 23]. Figure 1 shows the unit cell of $CeRu_2Al_{10}$ and the high symmetry points of the Brillouin zone.

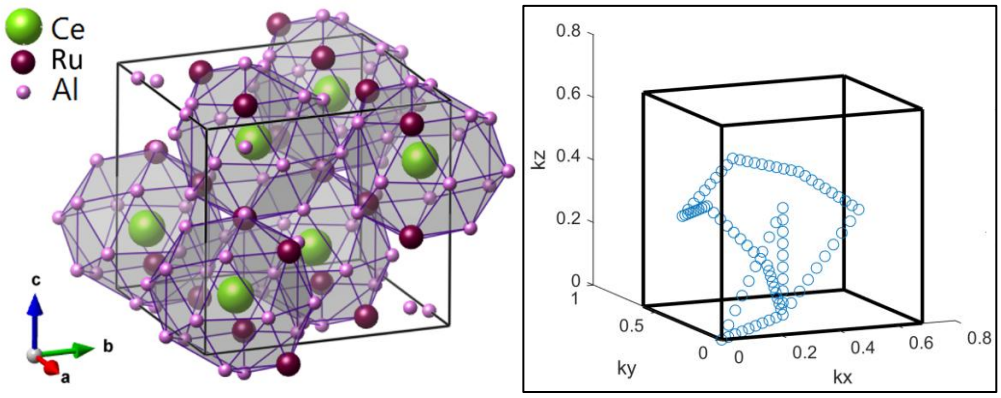


**Figure 1 The unit cell of $CeRu_2Al_{10}$ and the high symmetry points of the Brillouin zone.**

## 2.2 Muon Site Estimation

It was known that the most stable position for the $\mu^+$ to stop and interact with other magnetized ion was at the lowest potential energy inside the compound [24, 25]. By using the same exchange correlation functional, SIGMA = 0.2, LNONCOLLINEAR = TRUE and MAGMOM set to ± 1 $\mu_B$ antiferromagnetically along the *c*-axis, a SCF calculation was performed on 2 x 2 x 2 x 2 supercell to obtain the potential energy. The muon site location was determined by the coordinate of the lowest potential energy after the calculation was converged and reached the ground state energy.

## 2.3 Local Deformation

After the location of muon site was found, we performed a $\mu$SR simulation by inserting a $\mu^+$ at the position of estimated muon site. Since VASP didn't provide the pseudopotential of muon, we used the pseudopotential of hydrogen instead by changing the POMASS in the POTCAR file to be 1/9 of proton and added NELECT in INCAR file to simulate the $\mu^+$. Without fixing the coordinate and magnetic moment of each atom in the antiferromagnetic supercell structure, another SCF calculation was performed to let all the atoms and moments move and reach its equilibrium state. The initial magnetic moment was given as ± 1 $\mu_B$.

Received: August 04, 2025

International Journal of Applied Mathematics

Volume 38 No. 5, 2025

ISSN: 1311-1728 (printed version); ISSN: 1314-8060 (on-line version)

Two parts of calculation were performed which were ionic relaxation of an antiferromagnetic $CeRu_2Al_{10}$ supercell with and without $\mu^+$. All calculations were performed on 2 x 2 x 2 supercell. The position of all atoms and the value of magnetic moments were calculated until they converged.

## 4 Dipole Field Calculation

The dipole field originated from the interaction between the antiferromagnetic Ce-ions and random nuclear dipolar moments from all atoms inside $CeRu_2Al_{10}$. The dipole field interaction, $B_{\text{dipole}}$ experienced by the muon was contributed by the distance between the $\mu^+$ and the magnetic ions, the magnetic moments of the ordered magnetic phase, and the density of spin polarized electrons at the muon site. The dipole field was expressed as in Equation 1 where $\mu_0$ is the permeability of free space, $m_i$ is the magnetic moment of Ce-ions, and $r_i$ is the relative position between the muon and the $i^{\text{th}}$ Ce-ions.

$$B_{\text{dipole}}(r_\mu) = \frac{\mu_0}{4\pi} \sum_i \left( \frac{3r_i(m_i . r_i)}{r_i^5} - \frac{m_i}{r_i^3} \right) \qquad [1]$$

Since the local internal field perceived by the $\mu^+$ in $\mu$SR came from hundreds of unit cells, using the 2 x 2 x 2 supercell only couldn't give the accurate calculations. Although the periodic boundary condition used in DFT could simulate bulk material, the required supercell size to analyse the dipole field depends on the system. Generally, larger supercells were needed to minimize the interactions between the dipole and its periodic images which consequently allowed the calculation to converge. Besides, $CeRu_2Al_{10}$ experienced long-range interaction, thus a larger supercell was necessary.

Therefore, in order to achieve the total dipole field, the magnetization density was calculated over the volume of Lorentz sphere within the radius up to 100 Å or until the value was converged. Hence, two parts of calculation were performed during local deformation calculation.

After both parts of calculation were achieved, the results were combined so that the supercell with $\mu^+$ was surrounded by the supercell without muon in a Lorentz sphere as illustrated in Figure 2. The convergence test was done until the total dipole field was converged.

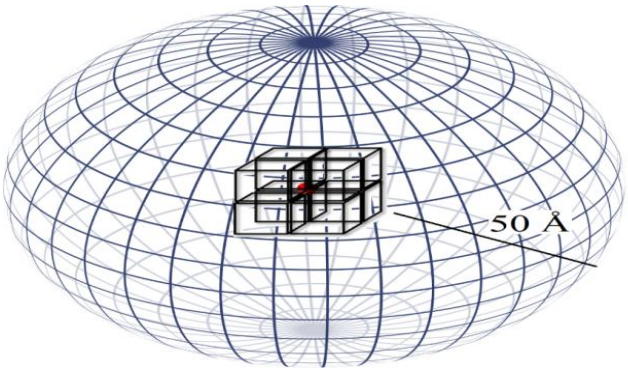


**Figure 2 Illustration of $\mu^+$ inside a 2 x 2 x 2 supercell within 50 Å of Lorentz sphere filled with pure $CeRu_2Al_{10}$ supercell.**

Received: August 04, 2025

International Journal of Applied Mathematics

Volume 38 No. 5, 2025

ISSN: 1311-1728 (printed version); ISSN: 1314-8060 (on-line version)

## 3.0 Results and Discussions

### 3.1 Band Structure

The energy of ground state obtained from the calculation was -2446.20 eV. Figure 3 shows the electronic band structure attained from the calculation. The density of state (DOS) and the electronic structure of $CeRu_2Al_{10}$ suggested a metallic state with low DOS where a small DOS of ~20 states/eV was observed at the Fermi level. After the band structure was enlarged as in Figure 4, the c-*f* hybridization together with the metallic behaviour were seen at the gamma point. Low occupation of 4*f*-orbital at the Fermi level also was observed where the *f*-electrons in both valence and conduction bands were localized and small hybridization between the *f*-electron and the conduction bands were found.

Compared to the experimental results, the electronic structure of $CeRu_2Al_{10}$ observed from the band structure calculation could explain the metallic ground state of $CeRu_2Al_{10}$ and the semiconducting behaviour that appeared after 2 GPa of pressure was applied [8, 26]. If pressure was applied to this density of state, semiconducting behaviour could be generated, and the *c-f* hybridization will be reduced.

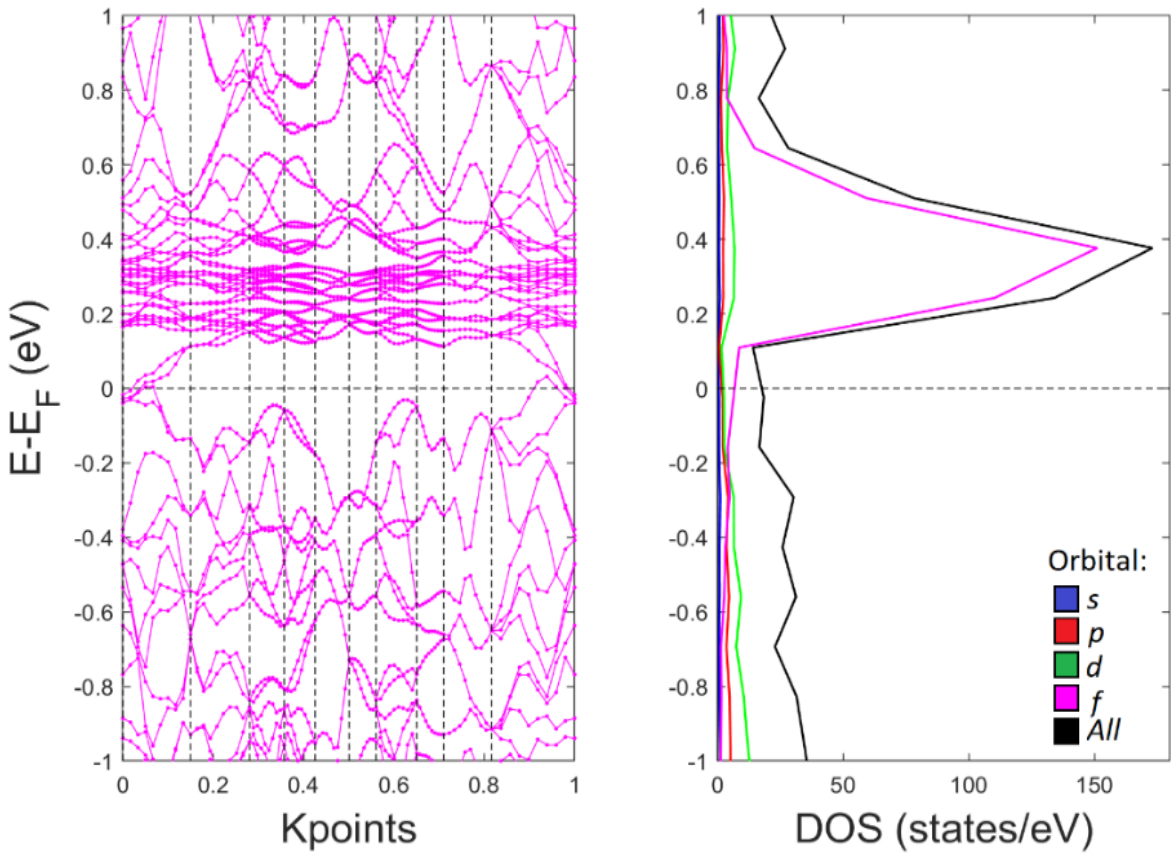


**Figure 3 The density of states and electronic band structure of $CeRu_2Al_{10}$ near the Fermi level.**

Received: August 04, 2025

International Journal of Applied Mathematics

Volume 38 No. 5, 2025

ISSN: 1311-1728 (printed version); ISSN: 1314-8060 (on-line version)

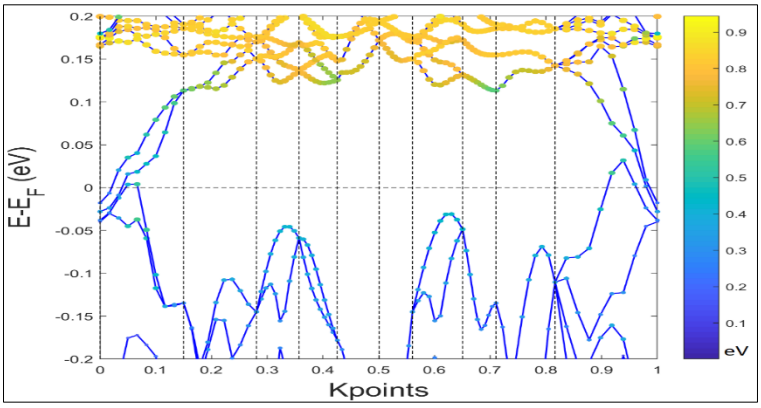


Figure 4 Low occupation of 4*f*-orbital denoted by the blue colour while yellow colour denoted the high occupation of 4*f*-orbital.

### 3.2 Muon Site Estimation

In order to locate the local minimum of electrostatic potentials, isosurface value of $\Delta V_0 = 100$ meV was applied using the VESTA [27]. The muon site was determined from the point where the lowest potential energy value resides, which was located at the fractional atomic coordinate (0.25, 0.50, 0.625) of a supercell with an energy of -12.003 eV. Compared to the estimated muon site analysed by Adroja *et al*. [16], it was located on the same crystallography site, only that this study estimated the muon site on a supercell. Therefore, we considered the calculated muon site to be in accordance with Adroja *et al*. The second muon site was located at (0.5, 0.5, 0.5) which was in accordance with Kambe *et al.* [14]. Figure 5 and Figure 6 show the image of crystallography planes where the lowest potential energy was observed in which will be called Adroja's site and Kambe's site, respectively. The estimated muon site is labelled with a positive black muon.

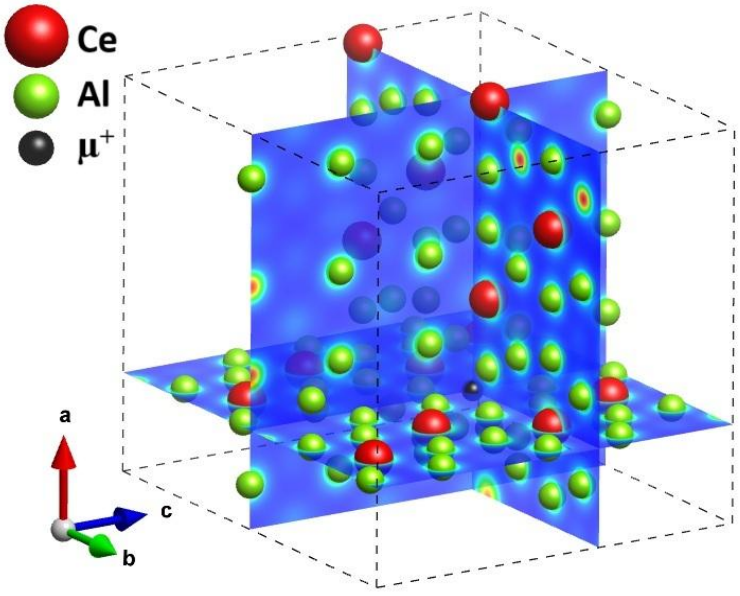


**Figure 5 The positions of Adroja's sites, (0.25, 0.50, 0.625).**

Received: August 04, 2025

International Journal of Applied Mathematics

Volume 38 No. 5, 2025

ISSN: 1311-1728 (printed version); ISSN: 1314-8060 (on-line version)

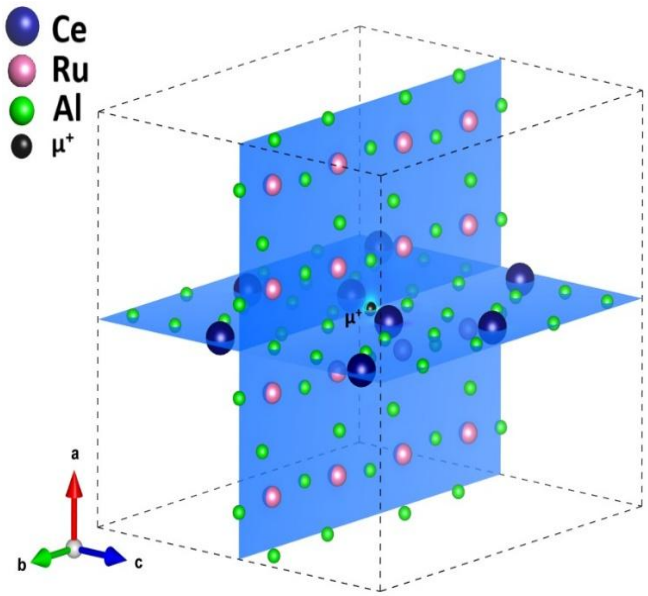


**Figure 6 The positions of Kambe's sites, (0.5, 0.5, 0.5).**

### 3.3 Local Deformation

After $\mu^+$ was inserted, all atoms and spins went through ionic and spin relaxation until they reached convergence state. Two sets of calculations were performed in which each set was inserted with a $\mu^+$ at Adroja's site and Kambe's site, respectively. The local deformation was observed. The $\mu^+$ together with other atoms near to it experienced a small displacement from the initial position.

#### 3.3.1 Adroja's Site

The final position of muon was (0.25, 0.5009, 0.6248) while the average displacement of all atoms was 0.0386 Å. The total energy was converged at -2466.258 eV which was 18.09 eV lower than without muon. In the supercell without $\mu^+$, the magnetic moment of Ce-ions converged to ± 0.353 $\mu_B$ which was lower than the experimental data, ± 0.42 $\mu_B$ [4]. But there were other experiments that also showed magnetic moments to be ±0.34 $\mu_B$ [13] and ± 0.38 $\mu_B$ [28]. Meanwhile, in the supercell with $\mu^+$, the magnetic moment increased to ± 0.5618 $\mu_B$. The $\mu^+$ not only affected the Ce-moments but also the Ru-atoms, which were initially non-magnetic. Figure 7 shows the difference of charge density between supercell with and without muon. From the charge density, it occurred that by adding the muon, the charge distribution of Ce and Ru were affected. Therefore, we suggested that the $\mu^+$ could have indirectly increased the hybridization between 4*f*-electrons of Ce with the conduction electrons of Ru and influenced the spin-orbit coupling behaviour.

Received: August 04, 2025

International Journal of Applied Mathematics

Volume 38 No. 5, 2025

ISSN: 1311-1728 (printed version); ISSN: 1314-8060 (on-line version)

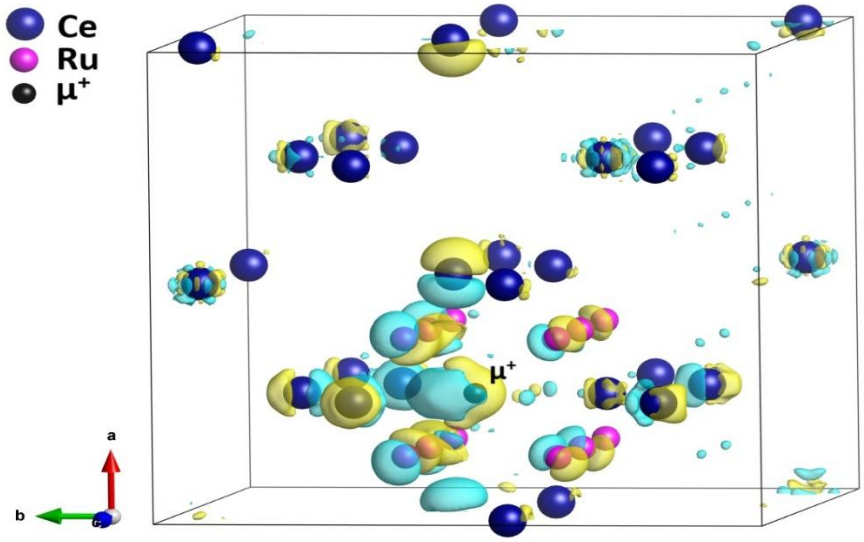


**Figure 7 The difference of charge density between supercell of $CeRu_2Al_{10}$ with and without $\mu^+$ at Adroja's site.**

### 3.3.2 Kambe's Site

The final position of muon was (0.5000 0.5001 0.5003) where the displacement of muon was only 0.0055 Å with average distance from Ce-ions, 2.6172 Å. The total energy with muon was converged lower at -2523.566 eV while the total energy without muon was -2448.239 eV. The total magnetic moment decreased to ± 0.015 $\mu_B$. The magnetization of Ce-ions reduced, and Ru-atoms also became magnetic. From the difference of charge density shown in Figure 8, the Ce and Ru were affected too but the area was bigger since the $\mu^+$ was positioned at the center of the supercell. However, the difference was smaller for each atom, and it was more localized compared to the Adroja's site. Thus, the magnetic moment became smaller than the experimental value.

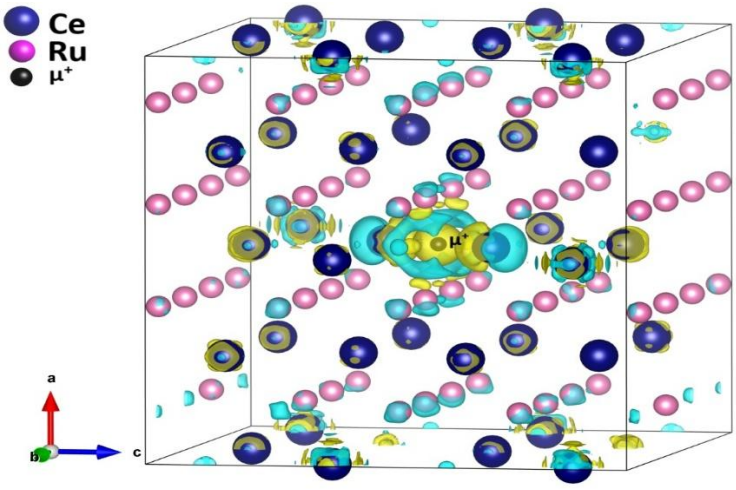


**Figure 8 The difference of charge density between supercell of $CeRu_2Al_{10}$ with and without $\mu^+$ at Kambe's site.**

Received: August 04, 2025

International Journal of Applied Mathematics

Volume 38 No. 5, 2025

ISSN: 1311-1728 (printed version); ISSN: 1314-8060 (on-line version)

### 3.4 Dipole Field

In order to verify the effect of $\mu^+$ towards the magnetized ions, dipole field calculation was done. Figure 9 shows the converged dipole field at 100 Å where the dipole field obtained from the estimated muon site was 151.8 G. The value was in the range within with the experimental values from $\mu$SR analysis of Khalyavin *et al* and Guo *et al* which were ~120 G and ~170 G [13,15]. Compared to Kambe's site, the converged dipole field at 100 Å was 21.5 G which was lower than experimental value, ~30 G. Figure 10 showed the convergence of dipole field at the muon site.

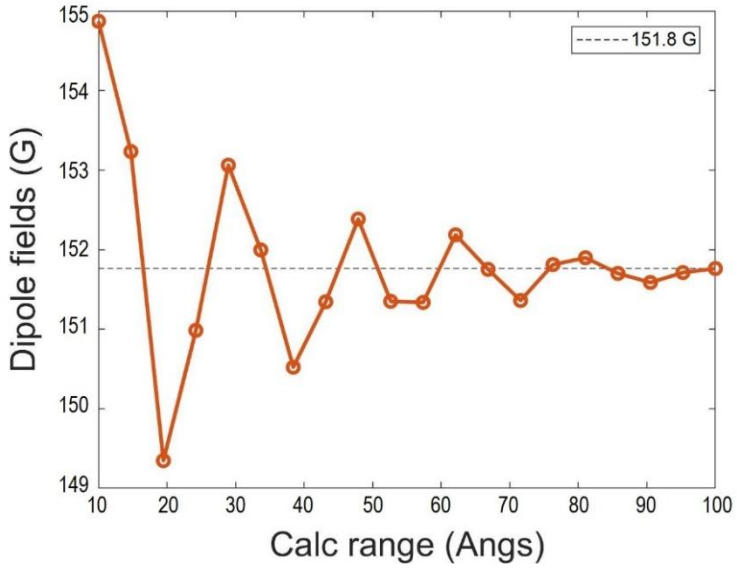


Figure 9 Convergence of dipole field at the Adroja's site.

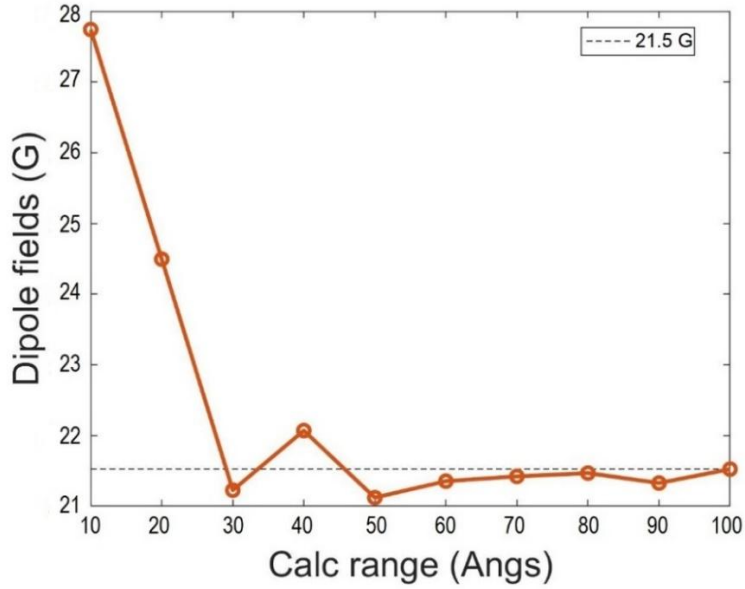


Figure 10 Convergence of dipole field at the Kambe's site.

Received: August 04, 2025

**International Journal of Applied Mathematics**

**Volume 38 No. 5, 2025**

ISSN: 1311-1728 (printed version); ISSN: 1314-8060 (on-line version)

## 4.0 Conclusion

In this study, we have simulated the metallic ground state of the antiferromagnetic $CeRu_2Al_{10}$ using 2 x 2 x 2 supercell and in the end, we have estimated the muon site and analyzed the dipole field. Throughout the calculation, we have deduced the electronic structure of $CeRu_2Al_{10}$ by taking the internal field from μSR analysis as our reference. From the observation, we suggested that the internal fields came from dynamic and static magnetic fields that arise from hybridization and ordered magnetic moments. Although the dipole field values were within the range of $\mu$SR experimental analysis, further analysis with different approaches such as adding Hubbard parameter or hybrid functional should be done to have better understanding of this sensitive material. Since $CeRu_2Al_{10}$ is highly sensitive to dopant and pressure, understanding the quantum phenomena of it would probably lead to future advancements in thermoelectric devices and technology.

## 5.0 Funding

This research received no specific grant from any funding agency in the public, commercial or not-for-profit sectors.

## 6.0 Acknowledgement

The author would like to acknowledge the use of supercomputer, HOKUSAI in RIKEN while performing this study. This study was supported by the International Program Associate (IPA) Program, RIKEN, Japan.

## 7.0 References

[1] Adroja, D. T., Hillier, A. D., Deen, P. P., Strydom, A. M., Muro, Y., Kajino, J., Kockelmann, W., Takabatake, T., Anand, V., & Stewart, J. (2010). Long-Range Ordering of Reduced Magnetic Moments in the Spin-Gap Compound $CeOs_2Al_{10}$ as Seen via Muon Spin Relaxation and Neutron Scattering. *Phys. Rev. B, 82*(10), 104405.

[2] Robert, J., Mignot, J.-M., Andre, G., Nishioka, T., Kobayashi, R., Matsumura, M., Tanida, H., Tanaka, D., & Sera, M. (2010). Long-Range Order and Low-Energy Magnetic Excitations in $CeRu_2Al_{10}$ Studied via Neutron Scattering. *Phys. Rev. B, 82*(10), 100404.

[3] Strydom, A. M. (2009). Thermal and Electronic Transport in $CeRu_2Al_{10}$: Evidence for a Metal-Insulator Transition. *Physica B, 404*(19), 2981 - 2984.

[4] Nishioka, T., Kawamura, Y., Takesaka, T., Kobayashi, R., Kato, H., Matsumura, M., Kodama, K., Matsubayashi, K., & Uwatoko, Y. (2009). Novel Phase Transition and the Pressure Effect in $YbFe_2Al_{10}$-type $CeT_2Al_{10}$ (T= Fe, Ru, Os). *J. Phys. Soc. Jpn., 78*(12), 123705.

[5] Matsumura, M., Tomita, N., Matsuoka, J., Kishimoto, Y., Kato, H., Kitagawa, K., Nishioka, T., Tanida, H., & Sera, M. (2014). Ru-NQR Study for Novel Phase Transition in $CeRu_2Al_{10}$. *J. Phys. Soc. Jpn., 83*(10), 103705.

[6] Muro, Y., Motoya, K., Saiga, Y., & Takabatake, T. (2010). Semiconducting Behaviour in $CeT_2Al_{10}$ (T= Fe and Ru). *J. Phys.: Conf. Ser., 200*, 012136.

Received: August 04, 2025

**Volume 38 No. 5, 2025**

ISSN: 1311-1728 (printed version); ISSN: 1314-8060 (on-line version)

[7] Kawabata, J., Ekino, T., Yamada, Y., Sakai, Y., Sugimoto, A., Muro, Y., & Takabatake, T. (2015). Hybridization Gaps and Antiferromagnetic Gap in the Kondo Semiconductors $CeT_2Al_{10}$ (T = Fe and Os) Oserved by Break-Junction Tunneling Spectroscopy. *Phys. Rev. B, 92*(20), 201113.

[8] Tanida, H., Nonaka, Y., Tanaka, D., Sera, M., Nishioka, T., & Matsumura, M. (2012). Anisotropic Pressure effect on the Electrical Resistivity of $CeRu_2Al_{10}$. *Phys. Rev. B, 86*(8), 085144.

[9] Kawamura, Y., Ogane, Y., Nishioka, T., Kato, H., Matsumura, M., Matsubayashi, K., & Uwatoko, Y. (2011). Magnetic and Transport Properties of $CeT_2Al_{10}$ (T= Fe, Ru, Os) Under Pressure. *J. Phys.: Conf. Ser., 273*, 012038.

[10] Matsumura, M., Inagaki, T., Kato, H., Nishioka, T., Tanida, H., & Sera, M. (2012). $^{27}$Al-NQR Study on Novel Phase Transition in $CeOs_2Al_{10}$. *J. Phys.: Conf. Ser., 400*, 032052.

[11] Matsumura, M., Tanida, H., Tanaka, D., Kato, H., Nishioka, T., & Sera, M. (2011). Reconciliation Between NQR Spectrum and Long-Range Magnetic Order in $CeRu_2Al_{10}$. *J. Phys. Soc. Jpn, 80*(8), 085001.

[12] Matsumura, M., Tomita, N., Matsuoka, J., Kishimoto, Y., Kato, H., Kitagawa, K., Nishioka, T., Tanida, H., & Sera, M. (2014). Ru-NQR Study for Novel Phase Transition in $CeRu_2Al_{10}$. *J. Phys. Soc. Jpn., 83*(10), 103705.

[13] Khalyavin, D. D., Hillier, A. D., Adroja, D. T., Strydom, A. M., Manuel, P., Chapon, L. C., Peratheepan, P., Knight, K., Deen, P., & Ritter, C. (2010b). Long-Range Magnetic Order in $CeRu_2Al_{10}$ Studied via Muon Spin Relaxation and Neutron Diffraction. *Phys. Rev. B., 82*, 100405.

[14] Kambe, S., Chudo, H., Tokunaga, Y., Koyama, T., Sakai, H., Ito, T. U., Ninomiya, K., Higemoto, W., Takesaka, T., & Nishioka, T. (2010). Evidence for Appearance of an Internal Field in the Ordered State of $CeRu_2Al_{10}$ by $\mu^+$SR. *J. Phys. Soc. Jpn, 79*(5), 053708.

[15] Guo, H., Tanida, H., Kobayashi, R., Kawasaki, I., Sera, M., Nishioka, T., Matsumura, M., Watanabe, I., & Xu, Z.-a. (2013). Magnetic Instability Induced by Rh Doping in the Kondo Semiconductor $CeRu_2Al_{10}$. *Phys. Rev. B, 88*(11), 115206.

[16] Adroja, D. T., Hillier, A. D., Deen, P. P., Strydom, A. M., Muro, Y., Kajino, J., Kockelmann, W., Takabatake, T., Anand, V., & Stewart, J. (2010). Long-Range Ordering of Reduced Magnetic Moments in the Spin-Gap Compound $CeOs_2Al_{10}$ as Seen via Muon Spin Relaxation and Neutron Scattering. *Phys. Rev. B, 82*(10), 104405.

[17] G. Kresse and J. Hafner, Phys. Rev. B 47 , 558 (1993); ibid. 49 , 14 251 (1994).

[18] G. Kresse and J. Furthmüller, Comput. Mat. Sci. 6 , 15 (1996).

[19] G. Kresse and J. Furthmüller, Phys. Rev. B 54 , 11 169 (1996).

Received: August 04, 2025 

**Volume 38 No. 5, 2025**

ISSN: 1311-1728 (printed version); ISSN: 1314-8060 (on-line version)

[20] Jain, A., Hautier, G., Moore, C. J., Ong, S. P., Fischer, C. C., Mueller, T., Persson, K. A., & Ceder, G. (2011). A high-throughput infrastructure for density functional theory calculations. *Computational Materials Science, 50*(8), 2295-2310.

[21] Setyawan, W., & Curtarolo, S. (2010). High-throughput Electronic Band Structure Calculations: Challenges and Tools. *Comput. Mater. Sci., 49*(2), 299 - 312.

[22] Thiede, V. M., Ebel, T., & Jeitschko, W. (1998). Ternary Aluminides $LnT_2$ $Al_{10}$ (Ln = Y, La-Nd, Sm, Gd-Lu and T= Fe, Ru, Os) with $YbFe_2$ $Al_{10}$ -type Structure and Magnetic Properties of the Iron-Containing Series. *J Mater Chem, 8*(1), 125 -130.

[23] Tursina, A. I., Nesterenko, S. N., Murashova, E. V., Chernyshev, I. V., Noel, H., & Seropegin, Y. D. (2005). $CeRu_2Al_{10}$ with the $YbFe_2Al_{10}$ structure type. *Acta Crystallogr, E61*(2), i12-i14.

[24] Bernardini, F., Bonfa, P., Massidda, S., & De Renzi, R. (2013). Ab Initio Strategy for Muon Site Assignment in Wide Band Gap Fluorides. *Phys. Rev. B, 87*(11), 115148.

[25] Bonfa , P., Sartori, F., & De Renzi, R. (2015). Efficient and Reliable Strategy for Identifying Muon Sites Based on the Double Adiabatic Approximation. *J. Phys. Chem. C, 119*(8), 4278 - 4285.

[26] Ishiga, T., Wakita, T., Yoshida, R., Okazaki, H., Tsubota, K., Sunagawa, M., Uenaka, K., Okada, K., Kumigashira, H., & Oshima, M. (2014). Electronic Structures of $CeM_2Al_{10}$ (M = Fe, Ru, and Os) Studied by Soft X-ray Resonant and High-Resolution Photoemission Spectroscopies. *J. Phys. Soc. Jpn, 83*(9), 094717.

[27] K. Momma and F. Izumi. (2011). VESTA 3 for Three-Dimensional Visualization of Crystal, Volumetric and Morphology Data. *J. Appl. Crystallogr., 44,* 1272-1276

[28] Strigari, F., Willers, T., Muro, Y., Yutani, K., Takabatake, T., Hu, Z., Chin, Y. Y., Agrestini, S., Lin, H. J., Chen, C. T., Tanaka, A., Haverkort, M. W., Tjeng, L. H. (2012). Crystal-field Ground State of the Orthorhombic Kondo Insulator $CeRu_2Al_{10}$. *Phys. Rev. B, 86*, 081105.

Received: August 04, 2025